Efficient Microwave Imaging Algorithm Based on Hybridization of the Linear Sampling and Level Set Methods

Ahmed M. Hassan, *Member, IEEE*, Tyler C. Bowman, *Student Member, IEEE*, and Magda El-Shenawee, *Senior Member, IEEE*

***Abstract*—A hybridized algorithm based on the linear sampling method and the level set technique is presented. The level set technique has shown the capability of accurate reconstruction of the shapes of unknown targets of different materials and arbitrary shapes but with significant computational time. The linear sampling method has shown comparatively rapid estimation of the targets' shapes. The presented algorithm retains the accuracy of the level set algorithm with significantly reduced computational time due to the hybridization of the level set method and the linear sampling method. Reconstruction results of Fresnel Institute experimental data are obtained using the hybridized algorithm.**

***Index Terms*—Inverse scattering problem, level set algorithm, linear sampling method, shape reconstruction.**

I. Introduction

SHAPE reconstruction algorithms have demonstrated several potential applications especially in medical imaging, nondestructive testing, geosciences, and airport security. Over the last decade, the linear sampling method (LSM) and the level set method have emerged as state-of-the-art methods in the field of shape reconstruction [1], [2].

The level set method, in general, is a mechanism to model/track evolving objects with high flexibility. The basic level set mechanism was developed by Osher and Sethian [3]. In the level set formulation, the evolving object is represented as the intersection of a higher order function with a constant value. This implicit representation facilitates the modeling of curves and corners as well as disconnected objects [3]–[5]. The level set technique has been incorporated in a plethora of applications such as image processing, computer vision, and computational physics [3]–[5]. Over the last decade, the level set method was implemented for microwave imaging of 2-D targets using TM and TE polarizations [6]–[10], reconstruction of experimental data [11]–[13], 3-D Perfect Electric Conductor (PEC) [14], 3-D dielectric targets of different materials [15], 3-D bacteria [16], and 2-D concealed targets hidden behind a wall [17]. In our previous works using the level set method, the method of moments (MoM) surface integral equation was used as the forward solver. The level set reconstruction results showed an excellent capability for accurate reconstruction of arbitrary shapes, even for multiple targets with different materials or targets hidden behind a dielectric wall [17]. However, the drawback was the intensive computational expenses as reported in [15]–[17]. One thought to reduce the computational time required by the level set algorithm was to implement the Message Parallel Interface (MPI) parallelization technique, since the level set algorithm is highly parallelizable. The parallelized level set algorithm has achieved a *speed up* to $\sim 100\times$ [18].

The LSM was first developed by Kirsh and Colton [2], [19]–[21]. Unlike the level set method, the LSM is a noniterative algorithm that reconstructs the shape of unknown targets with minimal *a priori* information. While the level set method requires the *a priori* knowledge of the electrical properties of the targets, the LSM does not require such knowledge. In addition, the LSM has shown significant speed in obtaining reasonable estimates of the unknown shapes [19]–[21]. Even though the LSM was initially invented through numerical experiments, several studies have proven and clarified the mechanism through which the LSM works [22].

Moreover, Catapano *et al.* have provided a physical interpretation to the LSM and linked this physical representation to the concepts of electromagnetic focusing [23]. The LSM was developed for the shape reconstruction of 2-D and 3-D targets, buried objects, cracks and arcs, and thin objects and screens [21]–[29]. Recently, the LSM algorithm was implemented to retrieve the dielectric permittivity of targets [29].

Based on our experience with the level set method, the convergence is guaranteed when a sufficient number of data at several incidents and receiving directions and frequencies is provided [15]–[17]. However, the LSM algorithm requires data collected at a number of incident and receiving directions greater than $2kR$, where k is the wave number and R is the minimum radius of the computational domain that encloses all unknown targets [21]–[29]. In other word, given a certain number of incident and receiving directions, there is a limit on the maximum frequency that can be utilized in the reconstruction using the LSM.

Manuscript received September 19, 2012; revised January 26, 2013; accepted March 09, 2013. Date of publication March 22, 2013; date of current version July 01, 2013. This work was supported in part by the Army Research Laboratory and was accomplished under Cooperative Agreement Number W911NF-10-2-0093 and in part by the MRI under Grants ARI #0963249, MRI #0959124, and EPS #0918970. The views and conclusions contained in this document are those of the authors and should not be interpreted as representing the official policies, either expressed or implied, of the Army Research Laboratory or the U.S. Government. The U.S. Government is authorized to reproduce and distribute reprints for Government purposes notwithstanding any copyright notation herein.

The authors are with the Electrical Engineering Department, University of Arkansas, Fayetteville, AR 72701 USA (e-mail: amhassan@uark.edu; tcbowman@uark.edu; magda@uark.edu).

Color versions of one or more of the figures in this paper are available online at http://ieeexplore.ieee.org.

Digital Object Identifier 10.1109/TAP.2013.2254444

The hybridization of the LSM with other algorithms was previously proposed to address the challenges of the inverse scattering problem [27], [28]. A hybrid, two-step imaging algorithm was developed by combining the LSM shape reconstruction algorithm with tomography algorithms such as the Optimized contrast source-extended Born (O-CS-EB) algorithm [27] and the Ant Colony Optimization (ACO) algorithm [28]. In [27], [28], the LSM was employed to reconstruct the shape of the target in the first step. In the second step, the knowledge of the shape was used to improve the accuracy of the reconstruction of the electrical properties in tomography. The goal of the current paper is a hybridization of the level set shape reconstruction algorithm with the LSM for the sake of speeding up the shape reconstruction. Therefore, unlike the previous reported hybridizations [27], [28], the LSM is not combined with a tomography algorithm but with another shape reconstruction algorithm, the level set, aiming to retain their complementary advantages.

In the hybridization of the LSM and level set algorithm, the output of the LSM reconstruction is used to initialize the level set algorithm. It is worth noting that there is some analogy between using the LSM to initialize the level set algorithm and the methods used to initialize tomography algorithms. In iterative tomography algorithms, an initial permittivity distribution is assumed in the imaging domain and is iteratively updated until the true permittivity distribution in the computational domain is reconstructed [30], [31]. Examples of methods for choosing the initial permittivity distributions are the 1st order Born Approximation [30] and backpropagation [31]. However, the hybridization developed in this paper uses the LSM contour, not a permittivity distribution, to initialize the level set algorithm.

For simplicity and to conduct a quantitative comparison, the work will be focused on 2-D homogeneous PEC targets immersed in air using both synthetic and experimental measurements data from the Fresnel Institute website [32], [33]. In this work, the transverse magnetic (TM) polarization is employed in the reconstruction results; however, a comparison between the TE and TM reconstruction using the level set algorithm was reported in [10]. While our preliminary synthetic reconstruction results based on the LSM were published in the conference paper [34], the current work presents the hybridization of the level set method with the LSM and the implementation on the experimental data.

This paper is organized as follows: brief discussions of the level set, the linear sampling method, and the hybridized algorithm are given in Section II. The synthetic and experimental reconstruction results obtained using the conventional level set, the conventional LSM, and the hybridized algorithm are presented in Sections III and IV, respectively, and conclusion remarks are given in Section V.

II. Shape Reconstruction Algorithms

In this Section, the main features of the level set and the LSM are summarized. The measurements are conducted at multiple frequencies and at multiple incident and receiving directions (see Fig. 1).

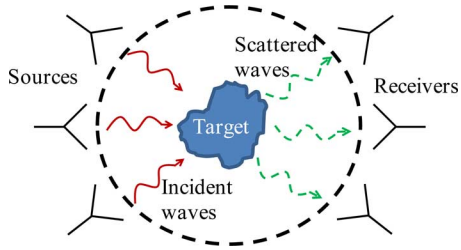

Fig. 1. Inverse scattering problem configuration.

A. Level Set Algorithm

The level set algorithm starts with an arbitrary initial guess that evolves to the true target. The evolving object is implicitly modeled as the zero level of a higher order function termed the level set function (details are given in [12]–[18]). Upon solving the following Hamilton Jacobi equation, the level set function φ is calculated at each pixel in the computational domain as follows:

$$\frac{\partial \varphi}{\partial t} + F(\bar{r})\|\nabla \varphi\| = 0, \quad \varphi_0 = \varphi(\bar{r}, t = 0) \tag{1}$$

where $F(\bar{r})$ is the *deformation velocity*, φ_0 are the initial values of the level set function, and $\bar{r}$ is the position vector. The level set function φ is zero on the contour or the surface of the evolving object. Equation (1) is discretized both temporally and spatially and is solved using the finite difference scheme where the level set function is updated at each spatial pixel and at each time iteration. For stability of (1), the Courant-Friedrichs-Lewy (CFL) condition requires that the numerical velocity, arising from the finite difference discretization, does not lag the physical speed. That is, $\Delta x/\Delta t$ has to be larger than the maximum value of the deformation velocity $F(\bar{r})$ in the entire domain. High resolution results can be obtained when fine spatial discretization, $(\Delta x, \Delta y)$, is employed in solving (1). In this case, reduction in the time step is necessary to satisfy the CFL stability condition [3]–[5]. As a result, larger number of inversion iteration will be required to achieve the algorithm convergence.

The deformation velocity is defined to decrease the difference between the measured fields scattered from the true targets and the fields scattered from the evolving objects [12]–[18]. This will ensure that the evolving object will converge to the true target. Hence, the deformation velocity $F(\bar{r})$ is expressed as shown in (2)

$$F(\bar{r}) = -\gamma \mathrm{Re}\Bigg(e^{-i\frac{\pi}{4}} \sum_{\theta^{\mathrm{inc}}} \sum_{\theta^{\mathrm{meas}}} \left(E_{\mathrm{evolving}}(\theta^{\mathrm{inc}}, \theta^{\mathrm{meas}}) - E_{\mathrm{meas}}(\theta^{\mathrm{inc}}, \theta^{\mathrm{meas}}) \right)^* J(\bar{r}) J'(\bar{r}) \Bigg) \tag{2}$$

[12]–[18]. In (2), γ is a constant to ensure stability; E_{evolving} are the far field patterns scattered from the evolving object; E_{meas} are the measured far field patterns scattered from the true target; θ^{inc} and θ^{meas} are the incident and scattered measurement directions, respectively; and $J(\bar{r})$ and $J'(\bar{r})$ are the forward and

adjoint surface current densities, respectively. The forward currents are induced due to the incident plane wave, while the adjoint currents are induced due to synthetic incident fields represented by the complex conjugate of the difference between the scattered and measurements field data (i.e. the back-propagation fields) [12]–[18]. The forward and adjoint surface current densities are calculated using the MoM solution of the Electric Field Integral Equation (EFIE). The computational burden of the level set method is due to the MoM calculations of the surface currents at multiple frequencies and for multiple incidences, while the updates of the level set functions do not represent major computational expenses.

A frequency hopping scheme is employed to provide multifrequency data, which improves the algorithm robustness against the nonlinearity and the ill-posedness of the inverse scattering problem, although there is no guarantee to avoid local minima. This multifrequency hopping technique has shown robustness of the level set algorithm in all our previous works [12]–[18]. Provided that an adequate number of frequencies are utilized, the level set algorithm always managed to converge to the true target regardless of the initial guess [12]–[18].

As known, the EFIE can cause a convergence issue if the operating frequency happens to be the interior resonance of the evolving object. However, we never encountered this issue in our previous microwave and higher frequency range works [12]–[18]. We believe that employing more than one frequency in the multifrequecny hopping scheme helps the algorithm to avoid the internal resonance problem of the EFIE formulation. In case a convergence issue occurs when using EFIE for PEC targets, the combined field integral equation can be used instead. In addition, other versions of the MoM were successfully implemented in our previous work, where the Poggio-Miller-Chang-Harrington-Wu (PMCHW) integral equation was implemented for dielectric targets [15].

B. Linear Sampling Method

The linear sampling method is based on solving the following far field Fredholm equation [19]–[29]:

$$\int_{\Omega} E_{\text{meas}}(\theta^{\text{meas}}, \theta^{\text{inc}}) g(\theta^{\text{inc}}, z) d\theta^{\text{inc}} = \Phi_{\infty}(\theta^{\text{meas}}, z) \quad (3)$$

where $E_{\text{meas}}(\theta^{\text{meas}}, \theta^{\text{inc}})$ is the far field pattern scattered from the unknown targets measured at a receiver angle θ^{meas} due to a plane wave excitation at angle θ^{inc}. The function $g(\theta^{\text{inc}}, z)$ is the unknown to be solved for at each pixel z in the imaging computational domain. The function $\Phi_{\infty}(\theta^{\text{meas}}, z)$ represents the far field pattern measured at an angle θ^{meas} due to a point source at z [19]–[29]. Equation (3) represents a linear system of equations to be solved to obtain $\|g(:, z)\|$ at all pixels z in the domain, where $\|\cdot\|$ is the norm operator. The linear system of equations of (3) is highly ill-conditioned and, therefore, Tikhonov regularization is typically implemented using a positive regularization parameter α [21]. In the original LSM implementation, Tikhonov regularization was implemented at each pixel and a different value of α was calculated at each pixel. Brignone *et al.* developed a no-sampling LSM adaptation where only one regularization parameter was calculated for the whole domain with similar results as the traditional LSM method [35]. In the current work, a single regularization parameter, $\alpha = 0.01\lambda$, is employed in the whole domain where λ is the wavelength in free space following the work in [23]. This value of α is not derived from the no-sampling approach but it is based on physical considerations as detailed in [23].

The values of $\|g(:, z)\|$ at pixels inside the unknown target are small compared with those outside the target region. The target can be reconstructed by designating a threshold between inside and outside the target region [19]–[29]. Different targets generate different ranges of $\|g(:, z)\|$. Therefore, the optimum threshold is usually defined relative to the maximum and minimum values of $\|g(:, z)\|$ for each target [26]. To the best of our knowledge, there is no rigorous theoretical analysis to suggest the optimum value of this threshold. The optimum relative threshold is typically estimated via reconstructing similar known targets, estimating the optimum relative threshold value for these known targets, and then applying this relative threshold in reconstructing the unknown targets [26].

A multiple frequencies LSM approach was reported in [25] where (3) is solved to obtain $\|g(:, z)\|$ at each frequency. The overall multiple frequencies $\|g_{MF}(:, z)\|$ is calculated as the normalized average of $\|g(:, z)\|$ at each frequency based on the following definition [25]:

$$\|g_{MF}(:, z)\| = \frac{1}{N_F} \sum_{f=1}^{N_F} \frac{\|g_f(:, z)\|}{\max \|g_f(:, z)\|} \quad (4)$$

where the summation over f represents the summation over the total number of frequencies N_F.

C. Hybridized Algorithm

In the hybrid algorithm, the LSM is first executed to obtain a relatively fast estimate of the location and shape of the unknown target. The LSM is typically conducted at low frequencies since its implementation requires a number of incident and receiver angles larger than $2kR$, where k is the wave number and R is the radius of the computational domain.

The principal idea is to use the LSM to rapidly estimate the contour and then use this contour as the initial guess for the level set algorithm. The initial guess will be now closer to the true target compared to unguided initial guesses, which will lead to a smaller number of inversion iterations in the level set algorithm. In the conventional level set algorithm the initial values of the level set function at each pixel in the domain are calculated using the signed distance [12]–[18]. In the hybridized algorithm, the signed distance at each pixel is defined as the minimum distance to the selected LSM contour to be used as the initial guess. The initial level set function is set to be negative for pixels inside the contour, positive for pixels outside the contour, and zero on the contour.

III. Synthetic Reconstruction Results

In this section, PEC 2-D targets are considered. In the first example, the star-shaped target shown as a solid blue contour in Fig. 2(b) is considered. The star-shape is particularly challenging because of its multiple length scales. This example is

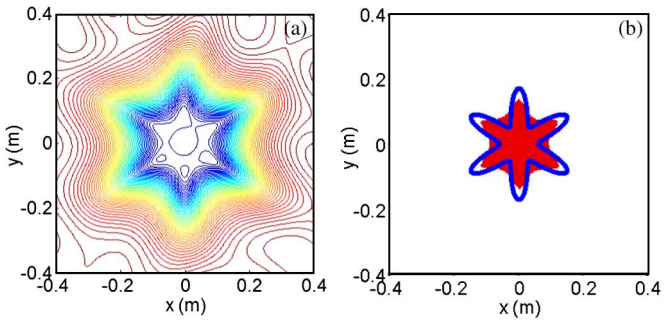

Fig. 2. Synthetic star-shaped target. (a) Single frequency 0.6 GHz, LSM contours corresponding to different values of $\log \|g(:,z)\|$ (b) The LSM optimum reconstruction achieved by selecting the best contour in Fig. 2(a). The true target is shown in solid blue contour, and the LSM reconstruction is shown as the filled red region.

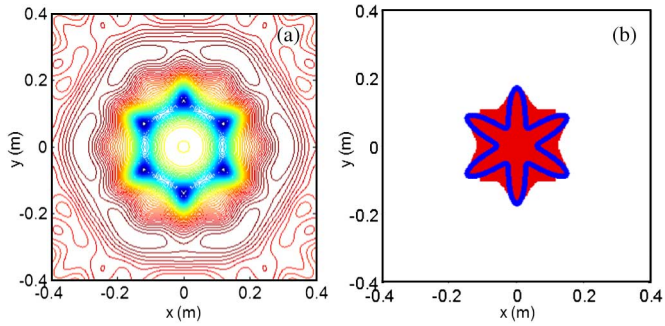

Fig. 3. Synthetic star-shaped target. (a) Average of multiple frequencies LSM contours corresponding to different values of $\log \|g_{MF}(:,z)\|$ (b) The LSM optimum reconstruction achieved by selecting the best contour in Fig. 3(a).

used to compare the performance of the conventional level set, the conventional LSM, and the hybridized algorithms. The performance metrics used in the comparison are the computational time and the reconstruction error. The reconstruction error is defined as follows [36]:

$$\text{Error} = \frac{1}{N_P}\left(\sum_{n=1}^{Nc} P\right) \times 100 \tag{5}$$

where N_p is the total number of pixels inside the true target, N_c is the total number of pixels in the computational domain, and P is set equal to 0 or 1 if a pixel is correctly or incorrectly classified, respectively. The conventional error function in shape reconstruction algorithms, known as the cost function, is defined by the difference between the electric fields scattered from the reconstructed object and from the true target as reported in previous works [12]–[18]. However, in the current paper, we implemented a different assessment metric at each pixel in the domain as defined in (5). This assessment metric is selected because it provides a direct comparison between the level set and the LSM algorithms, where the domain in each method is divided into the same number of pixels.

In this example, the computational domain ranges from -0.4 m to $+0.4$ m in both x- and y-directions. It is divided into 250 $\times$ 250 pixels. From our experience with the level set method [12]–[18], and as anticipated, we obtain good reconstruction results when the spatial discretization is comparable to the size of the fine features of the target. In the star example in Fig. 2, the computational domain was increasingly divided to reach 250 $\times$ 250 pixels which corresponds to a pixel size of 3.2 mm $\times$ 3.2 mm or $\lambda/15.6$ at 6 GHz which is the highest frequency employed (λ is the wavelength in air). These pixels are used to update the level set functions in the domain. Since the dimensions of the target are unknown, the number of pixels cannot be *a priori* known, but it can be obtained by progressively increasing the discretization. In both examples, the CFL stability condition was kept intact as discussed in (1). It is important to emphasize that the computational bottleneck of the level set algorithm is due to the MoM computations of the electric current densities and not due to the updates of the level set functions at each pixel in the domain [18]. Therefore, although the number of pixels in the domain is not changed with frequency, the MoM discretization of the evolving object is changed with frequency each time the algorithm hops to higher frequency in order to avoid over discretization and hence unnecessarily increase in the CPU and RAM requirements. In case the range of frequencies used in the hopping scheme become larger, it may be necessary to change the pixel size accordingly to avoid over discretization when updating the level set functions.

Twenty incident angles and twenty receiver angles uniformly distributed around the target are used. For this number of incident and receiver angles, the maximum frequency that can be employed successfully in the LSM algorithm is 1.5 GHz. However, there is no limit on the maximum frequency that can be employed in the level set algorithm either by itself or in the hybridized algorithm. The synthetic fields scattered from the target, calculated using the MoM, are corrupted with random noise according to the following formula [26]:

$$E^{\text{noise}}_{\text{meas}}(\theta^{\text{meas}},\theta^{\text{inc}}) = \left(1+0.1a(\theta^{\text{meas}},\theta^{\text{inc}})\right) E(\theta^{\text{meas}},\theta^{\text{inc}}) \tag{6}$$

where $a(\theta^{\text{meas}},\theta^{\text{inc}})$ is a random number ranging uniformly between -1 and $+1$. The random noise is added in (6) to avoid the inverse scattering crime. However, experimental measurements data are typically plagued with noise sources that are difficult to exactly emulate in synthetic data.

For the conventional LSM algorithm, eleven frequencies from 0.5 GHz to 1.5 GHz in steps of 0.1 GHz are utilized. The LSM algorithm is used to achieve the contour reconstruction at each frequency. Different frequencies provided different reconstruction accuracies, and the best accuracy was achieved using the frequency of 0.6 GHz (details are not shown here due to space limit). At this frequency, the various contours corresponding to different values of $\|g(:,z)\|$ are presented in Fig. 2(a). The values of the normalized $\|g(:,z)\|$ in Fig. 2(a) ranged from 0.005 to 0.8995 and the contour closest to the target is achieved at a value of $\|g(:,z)\|$ equal to 0.0069. The reconstruction from the best contour is shown in Fig. 2(b).

The average of the multiple frequencies LSM is shown in Fig. 3, where the various contours corresponding to different values of $\|g_{MF}(:,z)\|$ are presented in Fig. 3(a). The values of $\|g_{MF}(:,z)\|$ ranged from 0.0091 to 0.6545 and the contour closest to the target is achieved at a value of $\|g_{MF}(:,z)\|$ equal to 0.0364. The reconstruction from the best contour is shown

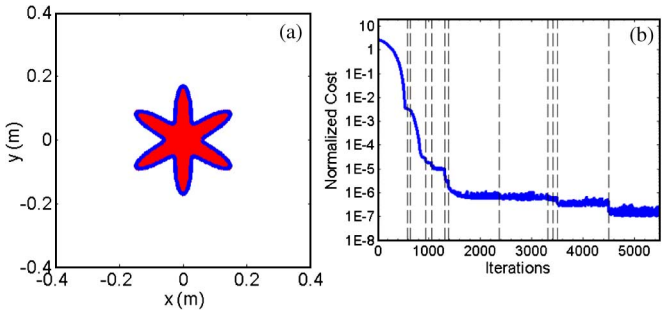

Fig. 4. Synthetic Star-shaped target, (a) final level set reconstruction of the star-shaped target using the frequency range 0.5 GHz to 6 GHz. The true target is shown in blue contour, while the reconstruction is shown as the filled red region. (b) The normalized cost function of the reconstruction (i.e. the error function). The dashed vertical lines indicate to where frequency hopping occurs.

TABLE I
SUMMARY OF RECONSTRUCTION TIME AND ERROR USING SYNTHETIC DATA OF STAR-SHAPED TARGET

Algorithm	CPU Time	Error
Conventional LSM (0.5-1.5GHZ)	0.33 minutes	76%
Conventional LSM (0.6GHZ)	0.03minutes	38%
Conventional Level Set (0.5-6GHZ)	24.2 hours	3.6%
Hybridized algorithm (0.5-6GHZ) using Initial Guess 1in Fig. 6a	20.4 hours	4.4%
Hybridized algorithm (0.5-6GHZ) using Initial Guess 2 in Fig. 6b	6.2 hours	4.5%
Hybridized algorithm (0.5-6GHZ) using Initial Guess 3 in Fig. 6c	12.8 hours	5.0%

in Fig. 3(b). The results of Fig. 2 (single frequency) and Fig. 3 (average of multiple frequencies) show qualitative estimates of the star-shaped target using the LSM.

For the conventional level set algorithm, twelve frequencies ranging from 0.5 GHz to 6 GHz in steps of 0.5 GHz are utilized. The hopping criterion is implemented when the cost function is unchanged within a threshold of 1% [15], [36]. The initial guess of a circle with radius 0.32 m located at the center of the computational domain is used. The final reconstruction is shown in Fig. 4(a) and the normalized cost function is plotted versus the number of iterations in Fig. 4(b).

As shown in Fig. 4(b), a total of 5496 iterations were necessary to accurately reconstruct the unknown target. Upon comparing Figs. 2 and 3 with Fig. 4, it is clear that the reconstruction accuracy improved significantly when using the level set algorithm versus the LSM. However, it is important to emphasize that this improvement is due to the fact that the level set algorithm has utilized higher frequencies than those used in the LSM. When the same frequencies employed in the LSM algorithm, i.e. 0.5 GHz to 1.5 GHz, were employed in the level set algorithm (results are not shown) the reconstruction error was $\sim$34%, which is comparable to the LSM reconstructions in Figs. 2 and 3 (see Table I).

Finally, for the hybridized LSM and level set algorithm, the estimated contour of the LSM obtained at 0.6 GHz of Fig. 2 is used as the initial guess for the level set algorithm. A frequency range of 0.5 GHz to 6 GHz is used in the level set part of the hybridized algorithm. Since the true target is unknown, it is a challenge to estimate an optimum value of $\|g(:,z)\|$ that defines which LSM contour minimizes the reconstruction error in (Figs. 2 and 3). As a result, the best LSM contour is *a priori* unknown. Therefore, we demonstrate here the effect of selecting nonoptimum LSM contours as initial guess for the level set algorithm. Three different contours, corresponding to three different values of $\|g(:,z)\|$ in Fig. 2(a), are used as the initial guess of the level set part. The results are shown in Fig. 5. These three contours correspond to $\|g(:,z)\|$ equal to 0.005, 0.0069, and 0.022, respectively. These values are selected from the lower range of $\|g(:,z)\|$ since the essence of the LSM algorithm is that the pixels inside the target have lower values of $\|g(:,z)\|$ than those outside the target. The results of Fig. 5 show that the level set algorithm is independent of the selected LSM contour as the initial guess and also is independent of whether the LSM contour was obtained using multiple contours as in Fig. 5(a) or single contour as in Fig. 5(b) and (c). The final reconstructions achieved using the hybridized algorithm is shown in Fig. 5(d)–(f), and the normalized cost function is plotted versus the number of iterations for each of the three initial guesses in Fig. 5(g)–(i). The results show that the three initial guesses in Fig. 5 required 4684, 2206, and 3560 iterations to converge compared to 5496 iterations in the conventional level set algorithm. The performance of the three algorithms is summarized in Table I. The results in Table I show that the conventional LSM algorithm is several orders of magnitude faster than the conventional level set algorithm. On the other hand, the conventional level set algorithm provides almost one order of magnitude better accuracy than the conventional LSM algorithm at the expense of the increased computational time. Therefore, the prime advantage of the hybridized algorithm is retaining the advantages of both techniques. Specifically, the proposed hybridized algorithm achieves the same accuracy as the conventional level set algorithm but with a significant reduction in the computational time (see Table I). All results of this work are obtained using a 2 $\times$ 6 MB cache, 2.66 GHz, and 1333 FSB processor on the Star of Arkansas supercomputer.

IV. EXPERIMENTAL RECONSTRUCTION RESULTS

The experimental measurements from the complex 2-D PEC U-shaped target, *uTM_shaped.exp*, are obtained from the Fresnel Institute database [32], [33].The same comparison of the previous example is repeated here using the level set, the LSM, and the hybridized algorithm. The target is shown as the solid blue contour in Fig. 6(b). The experimental measurements consisted of 36 incidents angles evenly distribute from 0° to 360° around the target and 49 receiver angles evenly distributed from 60° to 300° degrees as measured from the incident direction [32], [33]. Eight frequencies equally distributed from 2 GHz–16 GHz were measured. Two sets of measurements were presented in the *uTM_shaped.exp* file: (*i* measurements with the U-shaped target and (*ii*) measurements without the U-shaped target [32], [33]. The calibration of the measurements in the *uTM_shaped.exp* file is performed here in two steps. First the measurements without the target are subtracted from the measurements with the target to extract the signature of the target to achieve the parameter f_{scat}^{U} which is proportional to

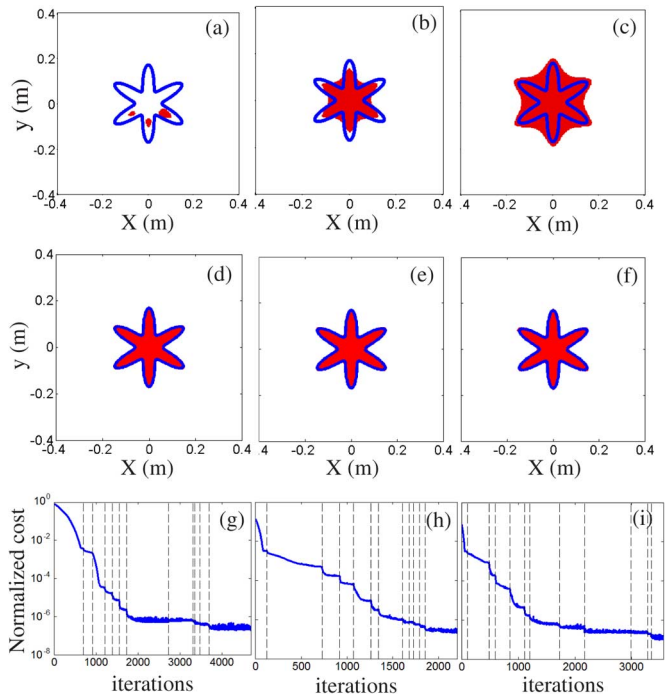

Fig. 5. Synthetic star-shaped target reconstructed using the hybridized LSM and level set algorithm (a) First initial guess correspond to LSM with $\|g(:,z)\| = 0.005$, (b) Second initial guess correspond to $\|g(:,z)\| = 0.0069$, (c) Third initial guess correspond to $\|g(:,z)\| = 0.022$; final reconstructions are shown in (d), (e), and (f), respectively. The normalized cost functions are shown in (g), (h), and (i) for the first, second, and third initial guess, respectively.

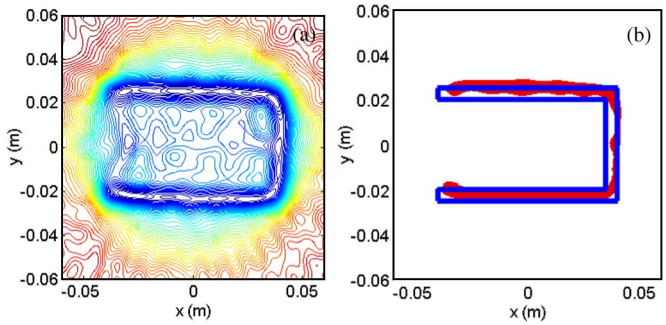

Fig. 6. Experimental U-shaped target (a) The LSM contours corresponding to different values of $\log\|g(:,z)\|$ (b) The LSM reconstruction achieved by selecting the best contour in Fig. 7(a).

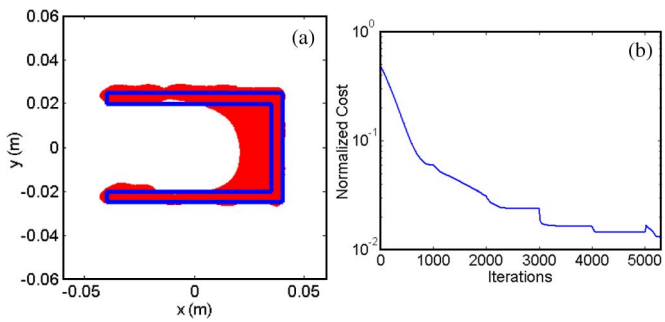

Fig. 7. Experimental U-shaped target, (a) final reconstruction using the conventional level set algorithm. The true target is shown in solid blue contour, while the reconstruction is shown as the filled red region. (b) The normalized cost function of the reconstruction.

the scattered fields. In the second step of calibration, a reference target is employed $f_{\text{scat}}^{\text{ref}}$ as follows [37], [38]:

$$E_{\text{scat}}^{U} = \frac{f_{\text{scat}}^{U}}{f_{\text{scat}}^{\text{ref}}} E_{\text{scat}}^{\text{ref}} \tag{7}$$

where E_{scat}^{U} is the calibrated scattered far field pattern of the U-shaped target, f_{scat}^{U} is the difference between the target and no target Fresnel measurements of the U-shaped target, $f_{\text{scat}}^{\text{ref}}$ is the difference between the target and no target Fresnel measurements of the reference target, and $E_{\text{scat}}^{\text{ref}}$ is the scattered far field pattern from the reference target calculated using an in house MoM code. The reference target measurements, $f_{\text{scat}}^{\text{ref}}$, used in this work are obtained from the *rectTM_dece.exp* file in the 2001 Institute Fresnel database. The file contains measurements from a 24.5 mm $\times$ 12.7 mm 2-D PEC rectangular target offset form the center of the computational domain [32], [33].

In the three algorithms, the computational domain ranges from -0.08 m to $+0.08$ m in both x- and y-directions. The thickness of the arm of the U-shaped target in Fig. 6 is 5 mm which is relatively thin. Therefore, the computational domain is discretized into a larger number of pixels, 400 $\times$ 400 pixels to capture the width of the U-shape. This discretization corresponds to a pixel size of 0.4 mm $\times$ 0.4 mm or $\lambda/46.8$ at 16 GHz which is the highest frequency employed. All the employed eight frequencies data, ranging from 2 GHz to 16 GHz, are used in the three reconstruction algorithms. For the conventional LSM algorithm, the average of all frequencies contours corresponding to $\|g_{MF}(:,z)\|$ are presented in Fig. 6(a) which ranges from 0.0848 to 0.65 with the contour closest to the target at $\|g_{MF}(:,z)\| = 0.1038$. The reconstruction using the LSM best contour is shown in Fig. 6(b). A 69% reconstruction error is calculated using (5) is achieved in this case. When a contour of $\|g_{MF}(:,z)\| = 0.095$ is selected instead of 0.1038, the reconstruction error increased to 77% (results not shown). For the conventional level set algorithm shown in Fig. 7, a total of 5300 iterations were necessary to obtain the final reconstruction of Fig. 7(a). The initial guess consisted of a 4 cm radius circle displaced by a distance of 1 cm to the right of the center of the computational domain. The hopping criterion is implemented when a fixed predetermined number of iterations is reached [16], [36]. In Fig. 7, the cost function hops to the consequent frequency after 1000 iterations for the first five frequencies and after 100 iterations for the last 3 frequencies. Another criterion was tested here which makes the algorithm hop to the other frequency when the cost function becomes unchanged within a threshold of 4%. We observed that the former stopping criterion provides slightly better results. As discussed in [36], a combination of stopping criteria can also be used to improve the results. The normalized cost function is plotted in Fig. 7(b) versus the number of iterations. The level set reconstruction in Fig. 7(a) successfully retrieved the location and the outer shape of the target but is not as accurate as the reconstruction achieved using synthetic data. In this case, a $\sim$114% reconstruction error, using (5), is achieved.

Finally, the results obtained using the hybrid algorithm are presented in Fig. 8. Two LSM initial guesses are used to test the hybrid algorithm. In the first case, the best LSM contour

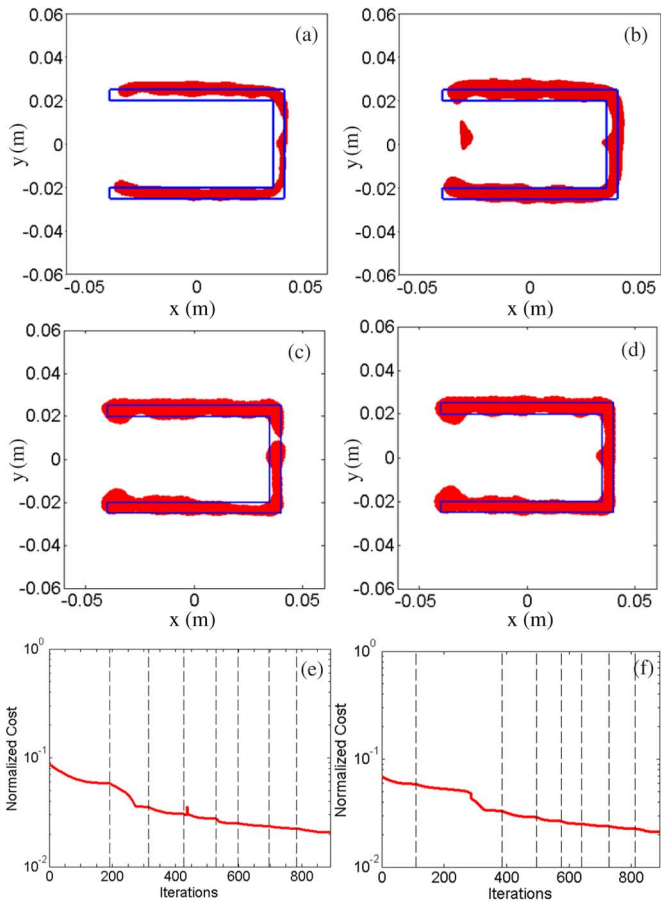

Fig. 8. Experimental U-shaped target, (a) first initial guess correspond to LSM with optimum $\|g(:,z)\| = 0.1038$, (b) Second initial guess correspond to nonoptimum $\|g(:,z)\| = 0.1187$; final reconstructions using the hybrid algorithm are shown in (c) and (d), respectively. The associated normalized cost functions of the hybridized algorithm are shown in Figs. 8(e) and (f), respectively.

used in Fig. 6(b) is utilized as the initial guess for the level set algorithm. The final reconstruction of the hybrid algorithm is shown in Fig. 8(c) and the corresponding normalized cost function versus the number of iterations is plotted in Fig. 8(e), respectively.

In this case, only 890 iterations are needed for the convergence of the level set algorithm (compared with 5300 iterations needed in Fig. 7). It should be noted that the same frequency hopping criteria is employed as in the conventional level set algorithm. The results demonstrate that the best final reconstruction of the U-Shape target is achieved using the hybridized algorithm upon comparing Figs. 6–8. A comparison is shown in Table II.

In the second example in Fig. 8, we demonstrate the effect of selecting a different LSM on the performance of the hybrid algorithm when implemented on the U-shape experimental measurement data of Fig. 7. We heuristically selected an initial guess from the LSM reconstruction contours corresponding to $\|g(:,z)\| \leq 1.4\min\{\|g(:,z)\|\}$. Notice that in Fig. 2 the best results are obtained when $\|g(:,z)\| = 0.0069$, which is $\approx 1.4\min\{\|g(:,z)\|\}$. The same heuristic selection is applied in this example. An initial guess corresponding to the best LSM

TABLE II
SUMMARY OF RECONSTRUCTION TIME AND ERROR USING EXPERIMENTAL DATA OF U-SHAPED TARGET USING 8 FREQUENCIES RANGING FROM 2–16 GHz

Algorithm	CPU Time	Error
Conventional LSM (2-16GHz)	1.7 minutes	69% (when best contour is *a priori* selected, Fig. 8a)
Conventional LSM (2-16GHz)	1.7 minutes	84% (using LSM contour of $\sim 1.4\times\min\{\|g(:,z)\|\}$ Fig. 8b)
Conventional Level Set (2-16GHz)	14.3 hours	114%
Hybridized algorithm (2-16GHz)	3.5 hours	56% (using best LSM contour of Fig. 8a)
Hybridized algorithm (2-16GHz)	4.8 hours	51% (using LSM contour of Fig. 8b)

contour $\|g(:,z)\| = 0.1038$ is shown in Fig. 8(a), and an initial guess corresponding to the LSM contour of $\|g(:,z)\| = 0.1187 \simeq 1.4\times 0.0848$ is shown in Fig. 8(b) $(\min\{\|g(:,z)\|\} = 0.0848)$. Notice the difference between the two initial guesses in Fig. 8(a) and (b), where a ghost shape appears in Fig. 8(b). The error in the conventional LSM reconstruction of the optimum contour shown in Fig. 8(a) is 69% versus the error of 84% in the nonoptimum contour of Fig. 8(b) as summarized in Table II. The results of Fig. 8(c) and (d) show the final reconstructions using the hybridized algorithm for the initial guess of Fig. 8(a) and (b), respectively. The associated normalized cost functions of the hybridized algorithm are shown in Fig. 8(e) and (f), respectively. Notice in Table II that when the nonoptimal initial guess is used, the hybridized reconstruction is still 3 times faster than the conventional level set algorithm and significantly more accurate than the conventional LSM. As anticipated, the reconstruction CPU time of the hybrid algorithm is ∼4.8 hours when the nonoptimal contour is selected, which is more than the ∼3.5 hours required when the optimum contour is selected.

Unlike the synthetic data example of the star-shape and other cases (not presented here for space limits), it is observed here that the conventional level set algorithm provided a higher reconstruction error compared with the conventional LSM algorithm. This observation could be due to the limited number of frequencies available in the 2001 Fresnel Institute measurements, which possibly limited the performance of the conventional level set algorithm. In all our previous work where synthetic data [14]–[18] or our experimental data [12], [13] was used, the final reconstruction using the level set algorithm was in very good agreement with the true targets; however, other metrics than (5) were calculated in [12]–[18].

In summary, the obtained results demonstrate that the LSM algorithm is significantly faster than the level set algorithm; however, the LSM has a constraint on the maximum frequency that can be employed. Also, there is no rigorous approach to select the best relative threshold for $\|g(:,z)\|$ in the LSM for the best contour selection. However, the results show that hybridizing the LSM with the level set algorithm mitigates these two limitations. In other words, the higher frequencies

that cannot be employed directly in the LSM, can be employed in the level set part of the hybridized algorithm. Also, if there was an error in selecting the LSM contour based on a relative threshold of $\|g(:,z)\|$, the level set part of the hybridized algorithm improves the reconstruction and mitigates the effect of this error.

On the other hand, the conventional level set algorithm uses an unguided selection of the initial guess which increases the computational time. Because the selected LSM contour is used as the initial guess, it is closer to the unknown contour of the target, and therefore the hybrid algorithm uses a smaller number of iterations to converge compared to the conventional level set algorithm.

The larger reconstruction error observed when the conventional level set algorithm is used to retrieve the U-Shape target using experimental data can also be attributed to the inherited drift noise in the data that may need additional signal processing to minimize its effect [12] and [39]. This noise might have caused the conventional level set algorithm, which employs an unguided initial guess, to get stuck at a local minimum. However, the hybrid algorithm was not affected as much by this noise because it started from an initial guess close to the target, and therefore it was able to escape from this local minima caused by the experimental noise. Therefore, hybridizing the LSM with the level set technique not only reduces the computational time of the reconstruction but it also improves its accuracy when other types of noise exist, especially in experimental data. Finally, the frequency hopping scheme used in the conventional level set algorithm was observed in previous works to affect the performance of the level set algorithm, but a reduction in that effect is noticed when hybridizing with the LSM.

V. Conclusion

While the LSM provides rapid shape estimation, more quantitative images are sometimes needed in applications such as medical imaging. Therefore, hybridization with the level set algorithm has demonstrated better accuracy and significantly reduced computational time when individually compared with each conventional algorithm. Although the reconstruction error and the CPU time shown in in Table II look better when the conventional LSM algorithm was used, they rely on the selection of the best contour which is not *a priori* known. On the other hand, and as shown in the star-shape example in Table I, neither the conventional level set algorithm nor the hybridized algorithm depend on the selection of the best contour. In this work, we demonstrated the advantages of the hybridized algorithm for 2-D PEC targets, but the work can be extended to 3-D dielectric targets in straightforward manner.

References

[1] M. Burger and S. Osher, "A survey on level set methods for inverse problems and optimal design," *Eur. J. Appl. Math.*, vol. 16, no. 02, pp. 263–301, 2005.

[2] D. Colton and A. Kirsch, "A simple method for solving inverse scattering problems in the resonance region," *Inv. Probl.*, vol. 12, no. 4, pp. 383–393, 1996.

[3] S. Osher and J. A. Sethian, "Fronts propagating with curvature-dependent speed: Algorithms based on hamilton--Jacobi formulations," *J. Computational Physics*, vol. 79, pp. 12–49, 1988.

[4] J. A. Sethian, *Level Set Methods and Fast Marching Methods*. Cambridge, U.K.: Cambridge Univ. Press, 1999.

[5] S. J. Osher and R. P. Fedkiw, *Level Set Methods and Dynamic Implicit Surfaces*. New York: Springer-Verlag, 2003.

[6] O. Dorn and D. Lesselier, "Level set methods for inverse scattering," *Inverse Probl.*, vol. 22, pp. R67–R131, 2006.

[7] R. Ferrayé, J. Dauvignac, and C. Pichot, "An inverse scattering method based on contour deformations by means of a level set method using frequency hopping technique," *IEEE Trans. Antennas Propagat.*, vol. 51, no. 5, pp. 1100–1113, May 2003.

[8] M. R. Hajihashemi and M. El-Shenawee, "Shape reconstruction using the level set method for microwave applications," *IEEE Antennas Wireless Propagat. Lett.*, vol. 7, no. 4, pp. 92–96, Apr. 2008.

[9] N. Irishina, M. Moscoso, and O. Dorn, "Microwave imaging for early breast cancer detection using a shape-based strategy," *IEEE Trans. Biomed. Eng.*, vol. 56, no. 4, pp. 1143–1153, Apr. 2009.

[10] M. R. Hajihashemi and M. El-Shenawee, "TE versus TM for the shape reconstruction of 2-D PEC targets using the level-set algorithm," *IEEE Trans. Geosci. Remote Sens.*, vol. 48, no. 3, pp. 1159–1168, May 2010.

[11] C. Ramananjaona, M. Lambert, and D. Lesselier, "Shape inversion from TM and TE real data by controlled evolution of level sets," *Inverse Probl.*, vol. 17, pp. 1585–1595, 2001.

[12] A. M. Hassan, M. Hajihashemi, M. El-Shenawee, A. Al-Zoubi, and A. Kishk, "Drift de-noising of experimental TE measurements for imaging of 2D PEC cylinder using the level set algorithm," *IEEE Antennas Wireless Propagat. Lett.*, vol. 8, pp. 1218–1222, 2009.

[13] D. A. Woten, M. R. Hajihashemi, A. M. Hassan, and M. El-Shenawee, "Experimental microwave validation of the level-set reconstruction algorithm," *IEEE Trans. Antennas Propagat.*, vol. 58, no. 1, pp. 230–233, Jan. 2010.

[14] M. R. Hajihashemi and M. El-Shenawee, "Inverse scattering of three-dimensional PEC objects using the level-set method," *Progr. Electromagn. Res.*, vol. 116, pp. 23–47, 2011.

[15] M. R. Hajihashemi and M. El-Shenawee, "Level set algorithm for shape reconstruction of non-overlapping three-dimensional penetrable targets," *IEEE Trans. Geosci. Remote Sens.*, vol. 50, no. 1, pp. 75–86, Jan. 2012.

[16] A. M. Hassan, M. R. Hajihashemi, and M. El-Shenawee, "Inverse scattering shape reconstruction of 3D bacteria using the level set algorithm," *Progr. Electromagn. Res. B*, vol. 39, pp. 39–53, 2012.

[17] M. R. Hajihashemi and M. El-Shenawee, "The level set shape reconstruction algorithm applied to 2D PEC targets hidden behind a wall," *Progr. Electromagn. Res. B*, vol. 25, pp. 131–154, 2010.

[18] M. R. Hajihashemi and M. El-Shenawee, "High performance computing of the level-set reconstruction algorithm," *J. Parallel Distrib. Comput. JPDC*, vol. 70, pp. 671–679, June 2010.

[19] D. D. Colton and P. Monk, "A linear sampling method for the detection of leukemia using microwaves," *SIAM J. Appl. Math.*, vol. 58, pp. 926–41, 1998.

[20] D. Colton, H. Haddar, and M. Piana, "The linear sampling method in inverse electromagnetic scattering theory," *Inverse Probl.*, vol. 19, pp. S105–S137, 2003.

[21] F. Cakoni, D. Colton, and P. Monk, *The Linear Sampling Method in Inverse Electromagnetic Scattering*. Philadelphia, PA: SIAM, 2011.

[22] T. Arens, "Why linear sampling works," *Inverse Probl.*, vol. 20, pp. 163–173, 2004.

[23] I. Catapano, L. Crocco, and T. Isernia, "On simple methods for shape reconstruction of unknown scatterers," *IEEE Trans. Antennas Propagat.*, vol. 55, no. 5, pp. 1431–1436, May 2007.

[24] G. Bozza, M. Brignone, and M. Pastorino, "Application of the no-sampling linear sampling method to breast cancer detection," *IEEE Trans. Biomed. Eng.*, vol. 57, no. 10, pp. 2525–2534, Oct. 2010.

[25] I. Catapano, L. Crocco, and T. Isernia, "Improved sampling methods for shape reconstruction of 3-D buried targets," *IEEE Trans. Geoscience Remote Sens.*, vol. 46, no. 10, pt. 2, pp. 3265–3273, Oct. 2008.

[26] D. Colton and P. Monk, "Target identification of coated objects," *IEEE Trans. Antennas Propagat.*, vol. 54, no. 4, pp. 1232–1242, Apr. 2006.

[27] I. Catapano, L. Crocco, M. D'Urso, and T. Isernia, "On the effect of support estimation and of a new model in 2-D inverse scattering problems," *IEEE Trans. Antennas Propagat.*, vol. 55, no. 6, pp. 1895–1899, Jun. 2007.

[28] M. Brignone, G. Bozza, A. Randazzo, M. Piana, and M. Pastorino, "A hybrid approach to 3D microwave imaging by using linear sampling and ACO," *IEEE Trans. Antennas Propagat.*, vol. 56, no. 10, pp. 3224–3232, Oct. 2008.
[29] L. Crocco, I. Catapano, L. Di Donato, and T. Isernia, "The linear sampling method as a way to quantitative inverse scattering," *IEEE Trans. Antennas Propagat.*, vol. 60, no. 4, pp. 1844–1853, Apr. 2012.
[30] Y. M. Wang and W. C. Chew, "An iterative solution of two-dimensional electromagnetic inverse scattering problem," *Int. J. Imag. Syst. Technol.*, vol. 1, pp. 100–108, 1989.
[31] R. E. Kleinman and P. M. van den Berg, "Two-dimensional location and shape reconstruction," *Radio Sci.*, vol. 29, no. 4, pp. 1157–1169, 1994.
[32] [Online]. Available: http://iopscience.iop.org/0266-5611/17/6/301/media
[33] K. Belkebir and M. Saillard, "Special section: Testing inversion algorithms against experimental data," *Inverse Probl.*, vol. 17, no. 6, pp. 1565–1571, 2001.
[34] A. M. Hassan, T. Bowman, and M. El-Shenawee, "The linear sampling method for the acceleration of the level set algorithm," presented at the IEEE Int. Symp. Antennas and Propag. and USNC/URSI National Radio Science Meeting, Chicago, IL, Jul. 8–13, 2012.
[35] M. Brignone, G. Bozza, R. Aramini, M. Pastorino, and M. Piana, "A fully no-sampling formulation of the linear sampling method for three-dimensional inverse electromagnetic scattering problems," *Inverse Probl.*, vol. 25, p. 015014, 2009.
[36] M. Benedetti, D. Lesselier, M. Lambert, and A. Massa, "A multi-resolution technique based on shape optimization for the reconstruction of homogeneous dielectric objects," *Inverse Probl.*, vol. 25, p. 015009, 2009.
[37] C. Gilmore, P. Mojabi, A. Zakaria, M. Ostadrahimi, C. Kaye, S. Noghanian, L. Shafai, S. Pistorius, and J. LoVetri, "A wideband microwave tomography system with a novel frequency selection procedure," *IEEE Trans. Biomed. Eng.*, vol. 57, no. 4, pp. 894–904, Apr. 2010.
[38] J. M. Geffrin and P. Sabouroux, "Continuing with the Fresnel database: Experimental setup and improvements in 3-D scattering measurements," *Inverse Probl.*, vol. 25, pp. 1–18, 2009.
[39] C. Eyraud, J. M. Geffrin, A. Litman, P. Sabouroux, and H. Giovannini, "Drift correction for scattering measurements," *Appl. Phys. Lett.*, vol. 89, p. 244104, 2006.

Ahmed M. Hassan (S'07–M'12) received the B.Sc. degree (with highest honors) and the M.Sc. degree both in electronics and communications engineering from Cairo University, Egypt, in 2004 and 2006, respectively, and the Ph.D. degree in electrical engineering from the University of Arkansas, Fayetteville, in 2010 in the bioelectromagnetics of breast cancer.

From 2004 to 2006, he was a Teaching Assistant at Cairo University, and from 2007 to 2010, he was a Teaching and Research Assistant in the Department of Electrical Engineering at the University of Arkansas. From 2011 to 2012, he was a Postdoctoral Fellow in the Computational Electromagnetics Group at the University of Arkansas. Currently, he is a guest researcher at the National Institute of Standards and Technology, Gaithersburg, MD. His current research interests include bioelectromagnetics, inverse scattering algorithms, nanoelectromagnetics, experimental microwave imaging, terahertz imaging, and metamaterials.

Dr. Hassan is the recipient of the Doctoral Academy Fellowship at the University of Arkansas.

Tyler C. Bowman (S'11) received the B.S. degree in electrical engineering from the University of Arkansas, Fayetteville, in 2012, graduating with highest honors. He is currently in a joint M.S./Ph.D. program at the University of Arkansas, with research primarily focused on inverse scattering algorithms for imaging and terahertz imaging applications as a graduate researcher in the Computational Electromagnetics Group.

In 2012, he also began working as a NSF GK-12 Fellow.

Magda El-Shenawee (M'91–SM'02) received the Ph.D. degree in electrical engineering from the University of Nebraska, Lincoln, in 1991.

After obtaining the Ph.D. degree, she joined the Center for Electro-Optics, University of Nebraska, as a Research Associate from 1992 to 1994, focusing on the enhanced backscatter phenomenon from random rough ground surfaces. She furthered her research at the National Research Center, Cairo, Egypt, from 1994 to 1996, then at the University of Illinois at Urbana-Champaign, Urbana, from 1997 to 1999. Directly before joining the University of Arkansas, Fayetteville, faculty, she served as a member of the Multidisciplinary University Research Initiative team working on the antipersonnel landmine detection at Northeastern University, Boston, MA, from 1999 to 2001. Currently, she is a Professor of electrical engineering with the University of Arkansas which she joined as an Assistant Professor in 2001. Her current research interests involve terahertz imaging and spectroscopy, computational inverse scattering algorithms, MEMS antennas, nano-antennas for energy enhancement of photovoltaic solar cells, and biomedical engineering applications to breast cancer using biopotentials and biological tumor growth modeling.

Dr. El-Shenawee is a member of Eta Kappa Nu electrical engineering honor society.